STREAM

IST-1999-10341

STREAM CONSORTIUM:
CNR-LAMEL / ST Microelectronics / ISEN / SOFT IMAGING SYSTEM / University of Sheffield / IMEC / CNR-IESS / University of Perugia

DELIVERABLE D20

Workpackage WP3

Lead participant: USFD
Partners: CNR-LAMEL, ST, USFD

Evaluation of advantages of 1 nm spatial resolution TEM/FEG techniques

Main Author	A.Benedetti, A.G. Cullis, USFD		
Contributing authors	A. Armigliato, R. Balboni, S.Frabboni, CNR-LAMEL; G.Pavia (ST)		
Date:	29 - 03 - 2002	***Doc.No:***	IST10341-USFD-RP001
Keywords:	Field emission guns, electron energy-filtering, convergent beam electron diffraction, spatial resolution		

Distribution list	**Project Officer:** B.Netange **Reviewers:** H.Cerva, S.Jones **All Partners:** G.P.Carnevale ST Microelectronics V. Senez ISEN T. Schilling Soft Imaging System A.Armigliato CNR-LAMEL I. De Wolf IMEC S. Lagomarsino CNR-IESS G. Carlotti UniPg (University of Perugia)

Table of contents

Introduction

The TEM/CBED activity in the STREAM project has been carried out with the electron microscopes available in the laboratories of the three partners CNR-LAMEL, ST and USFD. They differ from each other as to both the electron source (thermionic or field emission (FEG)) and the electron energy filtering capabilities. During this 2 year period CNR-LAMEL has updated its TEM facility, purchasing a new microscope, now equipped with a FEG source; it has become operating in July 2001 and it is employed also for the CBED analysis required by the project.

In this report the advantages for the strain analysis of using 1 nm electron spots obtainable with the FEG sources, over the 10 nm ones available in the LaB_6 equipped TEMs (like the one of ST and the previous microscope of CNR-LAMEL) will be assessed. The results complement those preliminarly described in Deliverable D5.

In addition, it has been found that electron energy filtering is of great use in the CBED work. It allows the strain analysis to be performed at room temperature with a clear advantage over the more common experiments carried out at low temperature (usually 100 K) by special cooling sample holders.

To this Deliverable two Appendices are appended. Appendix I deals with a preliminary CBED work in a new zone axis, namely the <150>, which can be applied to the strain analysis in plan sections or in <100> cross sections like in vertical transistors. Appendix II discusses the applicability of the <230> CBED analysis to the case of GaAs, which, though less important than silicon, is also a material of interest to the field of microelectronics; in fact, the partner SIS has received expressions of interest from the GaAs community for a suitable version of the CBED software.

1 Field Emission Guns (FEGs)

The illumination system of a modern TEM includes an electron source and a number of condenser lenses. The main design parameter of a gun is the brightness *B*, defined as the current density per unit solid angle ($A/cm^2/sr$). This factor determines the total current that can be focused on a specimen, which is the key parameter for the use of very small probes in CBED experiments. As *B* depends on the acceleration voltage *V*, it is convenient to work with the so-called reduced brightness $B_R = B/V$. The theoretical maximum electron intensity I_{th} is related to the brightness B_R through the equation:

$$I_{th} = B_R(\pi a^2 d^2 / 4)$$

where α is the semiangle of the probe-forming lens and *d* the diameter of the source.

There are two types of electron sources: the lanthanum hexaboride (LaB_6) single crystal and the field emission gun (FEG). In the former case, the electron beam is obtained by thermionic effect, then accelerated and focused in a crossover by a set of magnetic lenses. Tungsten or more often LaB_6 are normally used as thermionic sources, yielding brightness about 10^9 -10^{10} Am^{-2} sr^{-1}.

An alternative electron source is represented by the Field Emission Gun (FEG), in which electrons are originated by field emission from a microscopic W point. The thermal (or Schottky) FEG, which consists of a zirconiated W filament, is presently more commonly used than the cold FEG.

A FEG source yields a much higher brightness (10^{12} -10^{13} Am^{-2} sr^{-1}) and a very small emission area, which results in an intense enough signal even with a probe as small as 0.5 nm and an extremely small energy spread (typically less than 1 eV for the 200 kV TEMs). However, a very high vacuum ($P < 10^{-10}$ Torr) is required.

The USFD JEOL 2010F and the CNR-LAMEL Tecnai F20, pictured in Fig. 1.1 below, are both equipped with a FEG electron source, which renders CBED analysis with probe sizes ≤ 1 nm feasible.

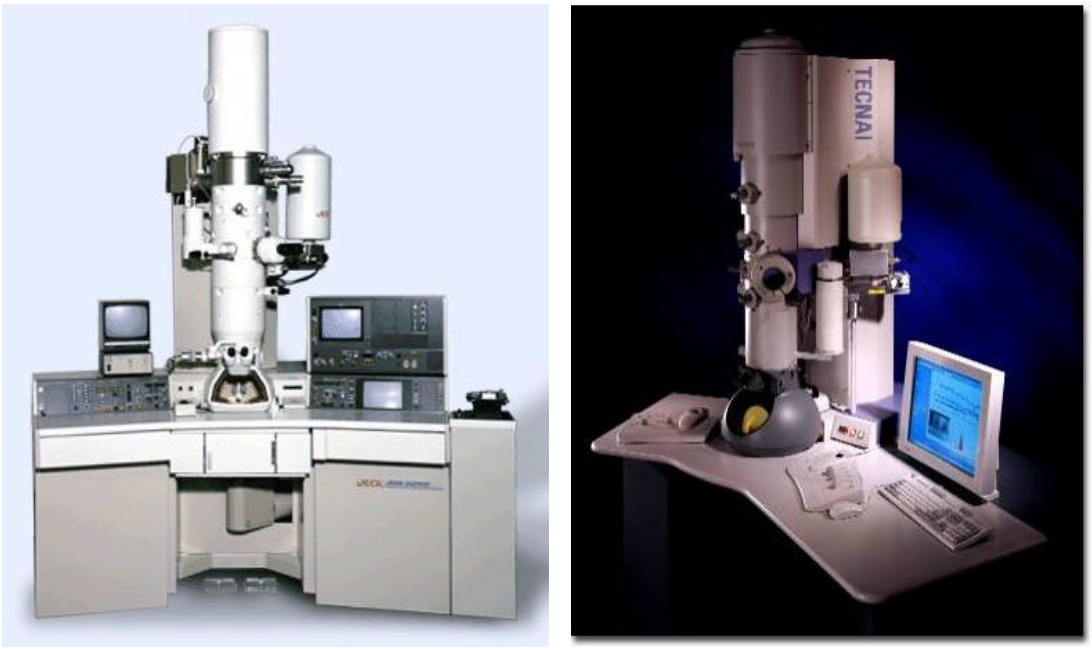

Fig. 1.1 – The JEOL 2010F (left) and the Tecnai F20 (right) available at the USFD and CNR-LAMEL facilities, respectively.

1.1. Contamination problems

The use of a FEG electron source for CBED analysis offers a number of advantages, as will be discussed in the next paragraph. The only partial drawback is represented by local overheating of the specimen, which in turn increases the presence of contamination on the sample surface mostly due to hydrocarbons released from it within the TEM column and locally redeposited by the beam. This effect blurs out CBED patterns by decreasing the peak-to-background ratio of the HOLZ lines, and worsens as the probe dimension is reduced.

An example can be seen in Fig. 1.2 below, where two CBED patterns from the same undistorted silicon area are shown. The blurring effects of contamination are clear when a 1 nm probe is used (left pattern), whereas the right pattern (acquired with a 4 nm probe) exhibits a much better S/N ratio. Both patterns were obtained with the Tecnai F20 microscope in Bologna.

Since the presence of contamination depends to an extent on the cleanliness of the sample surface and on the level of vacuum, this negative effect can be partly reduced by careful sample thinning and frequent bake-outs of the microscope.

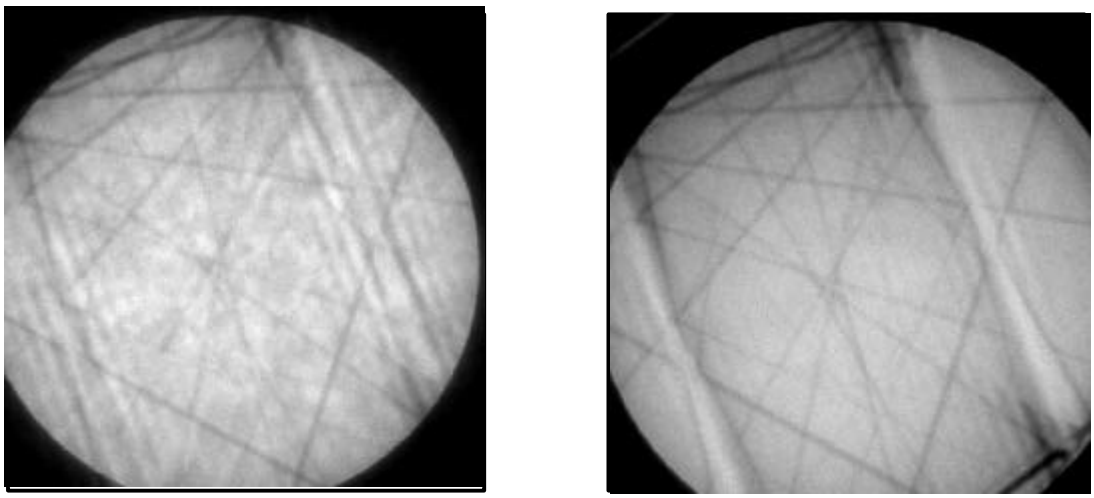

Fig. 1.2 – CBED patterns from undistorted silicon, acquired using a 1 nm **(left)** and a 4 nm **(right)** probe

1.2. Advantages of 1 nm spot size

The spatial resolution in CBED depends mainly on the probe size, as the HOLZ lines originate from a column of material whose diameter is roughly that of the incident beam. Therefore, whenever the strain distribution is markedly changing on the nanometer scale the use of a relatively large (~ 10 nm or larger) probe results in a blurred pattern, which cannot be analysed. This point was already mentioned in Deliverable 5 and experimentally studied in some devices of the 1st campaign[1]

In that work, we found that using the 1 nm probe allowed by the JEOL 2010F we were able to measure strain in a region as close to the oxide/active area interface as 30 nm, whereas the Philips CM30 then operating at LAMEL could only yield blurred patterns with a ~ 10 nm probe. In such regions, where the strain field rapidly vary within few nanometers, the use of a 1 nm probe is therefore recommended.

This result has been recently confirmed by a set of measurements performed with the Tecnai F20 at LAMEL, recording high quality CBED patterns at z ~ 40 –50 nm, employing LN_2 cooling but no filtering. The zone axis is the <230>, whereas in Deliverable D5 the experiments were performed in <130>; the acceleration voltage is 200 kV, instead of 100 kV. Two examples of these CBED patterns are reported in Fig. 1.3, showing perfectly visible HOLZ lines and a very good S/N ratio, particularly compared to that reported in Ref.1. Fig. 1.4 indicates where the patterns were acquired.

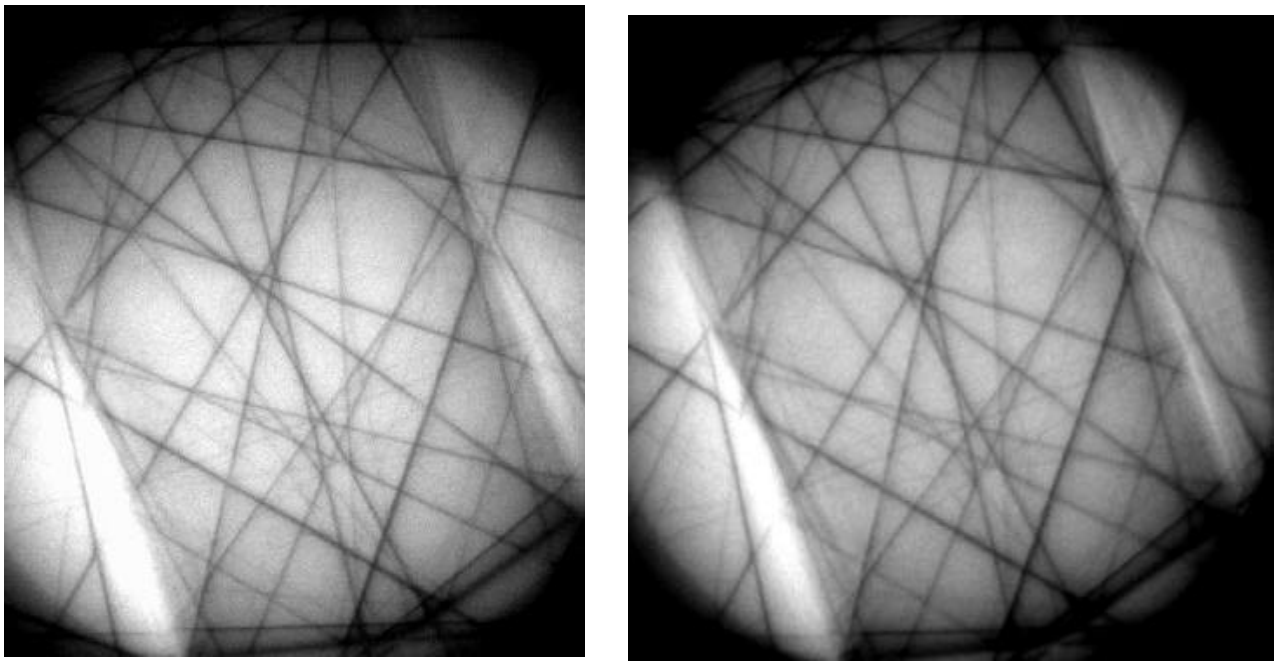

Fig. 1.3 – CBED patterns acquired with the Tecnai F20 in the points labelled A (left) and B (right) in Fig.1.4. Probe size: 1nm, LN_2-cooled sample

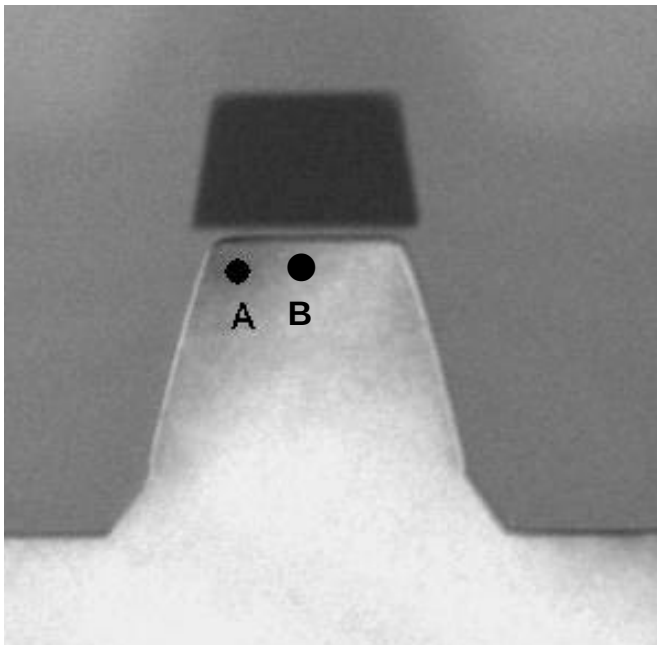

Fig. 1.4 – BF image of a device from wafer 7_4 from the 1st campaign; the dots indicate the positions where the patterns in Fig. 1.3 have been recorded.

The strain tensor in points A and B in Fig. 1.4 was calculated from the correspondent patterns using the AnalySIS_software. The results, reported in Table 1, show that the

deformation is markedly varying from the centre to the edge of the structure. In particular, the ε_{ZZ} component change by about a factor of three: this confirms that the regions with large strain gradients are better probed with a 1 nm electron spot.

Table I. Components of the strain tensor (incl. trace) obtained by CBED analysis of the patterns in Fig.1.3; distance from the padoxide/silicon interface: 40 nm

Pattern	**Position (x)**	**ε_{XX} * 10-4**	**ε_{ZZ}* 10-4**	**ε_{XZ} * 10-4**	**Tr(ε) *10-4**	**χ^2**
A	-110	0	6	-3.4	6	0.13
B	0	-2	17	-3.4	13	0.19

2 Specimen cooling

Using a liquid nitrogen (briefly, LN_2) cooled sample holder it is possible to achieve temperatures in the sample region close to 100 K. As it is well known, this greatly improves the quality of the experimental patterns, in terms of both lines visibility and S/N ratio. This is due to the fact that the CBED analysis employs High Order Laue Zones (HOLZ) rather than Zero Order Laue Zones (ZOLZ) lines; . The former originate from planes with higher Miller indices, hence are more sensitive to thermal diffuse scattering (which is proportional to the summed squares of the Miller indices). Therefore, lowering sample temperature greatly reduces the contribution of this factor. In addition, the effects of contamination by the beam-induced specimen heating are minimised, considerably improving the quality of patterns. For these reasons, LN_2-cooled sample holders are commonly used for CBED analysis.

However, there are a number of drawbacks related to sample cooling. First, the different components of the devices have different elastic constants, and would therefore expand or compress differently when cooled. This in turn may introduce a further factor to account for when measuring the strain components. However, it has been experimentally demonstrated that the differences in the thermal dilatation coefficient among Si, SiO_2 and Si_3N_4 decrease with decreasing the temperature, from room temperature to 100 K. This indicates that the strain analysis can be performed

also at low temperature without a significant reduction of accuracy, as reported in Deliverable D8.

Secondly, the following practical disadvantages have to be considered:

1- A specifically designed sample holder is necessary, in which the specimen is cooled by conduction from an insulated dewar. Therefore, the weight and dimension of this holder are largely exceeding those of a normal double-tilt holder, used for room temperature CBED experiments. The temperature is monitored by a calibrated silicon diode. Fig. 2.1 pictures a Gatan LN_2 cooled sample holder.

Fig. 2.1 – An LN_2 cooled TEM sample holder from Gatan Inc. The dewar to be filled with the liquid nitrogen is visible on the right. The thermal isolation is obtained by evacuating through a zeolite pump the space between the outer and the inner walls of the dewar.

2- This type of holders normally provides a much lower tilting range than conventional holders, if the objective lens is equipped with ultra-high resolution pole pieces. For instance, the holder of the JEOL 2010F available at USFD allows one to tilt up to ± 27° (around the goniometer axis), whereas that for specimen cooling can only reach ~ ±15°. The Tecnai F20 installed at LAMEL, however, having a Supertwin (not Ultratwin) objective lens, allows tilting to up to ~ ±35°. This is particularly important when analysis at a high tilt zone axis, such as <130>, is to be performed. Obviously, the point-to-point resolution of this latter configuration is somewhat lower.

3- Specimen cooling is rather time consuming, in which it takes around 1-1.5 hours before 100 K are reached and stabilisation is achieved. In addition,

further time is spent to warm the holder up to room temperature at the end of each session, thus reducing sample throughput.

4- Even when the temperature has stabilised, specimen drifting and/or vibrations within the holder may occur, as a result of the thermal gradients and the bubbling of the LN_2.

3 Energy-Filtering

3.1 Types of filters

Although energy-filtering is achieved in both JEOL 2010F and LEO 922 microscopes by a combination of magnetic prisms, the two systems are based on different geometries.

The LEO 922 of ST has an in-column-filter, which employs four magnetic prisms to energy-disperse and deflect the beam downwards along the optical axis. Due to the arrangement of the magnetic sectors, this filter is also called Ω-filter. The first order aberrations are fully corrected, due to the symmetry of the coils geometry; moreover, no alignment procedure is requested to the user.

The JEOL 2010F of USFD has a post-column energy filter, equipped with a CCD multiscan camera for filtered images. Here, a magnetic field orthogonal to the beam direction energy-disperses, deflects and focuses the beam on the detector. The latter system has an advantage over the former in that it can be easily attached to any conventional TEM; also, the energy dispersion is fairly linear over a range of several thousands eV. A drawback is given by the relatively low dispersive power, which means that some post-spectrometer magnifying optics has to be used to achieve a good energy resolution. The arrangement of these two spectrometers are sketched in Figure 3.1

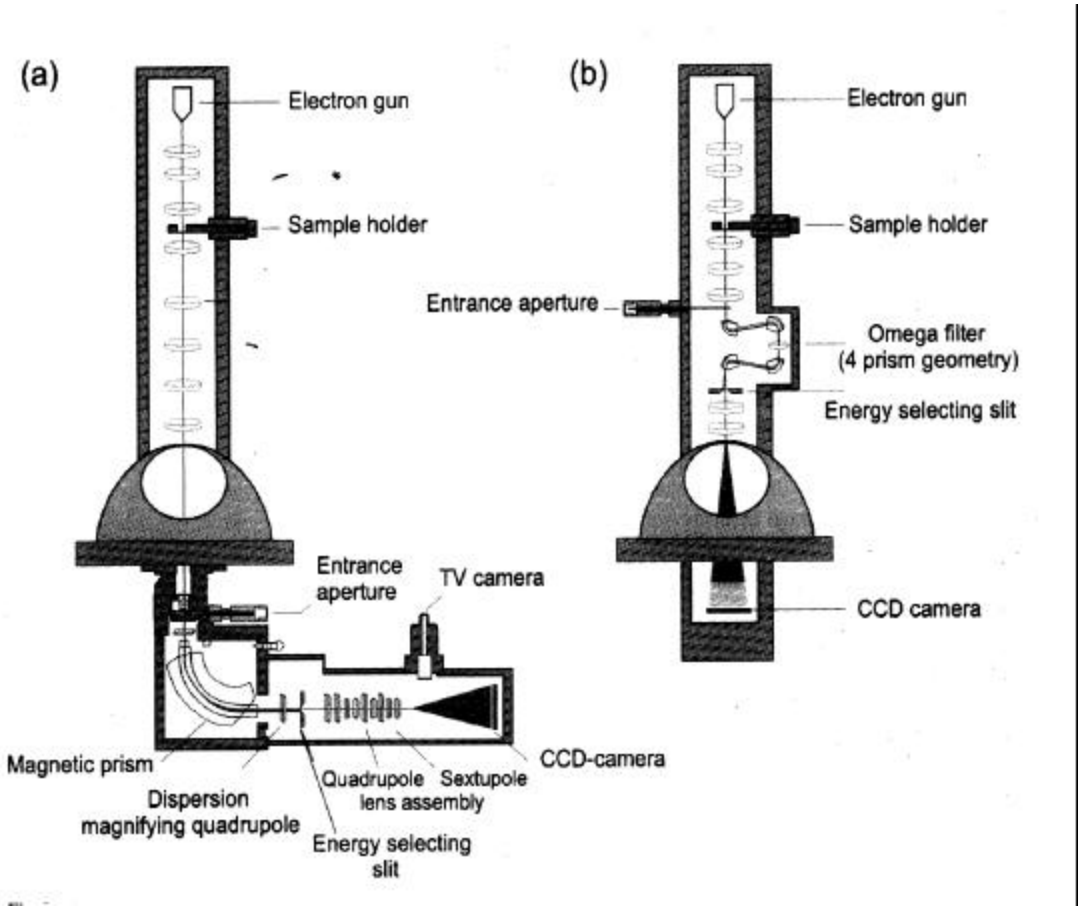

Fig. 3.1 - The two main types of energy-filters: the Gatan, post-column GIF system **(a)** and the LEO, in-column Ω filter **(b)**[2]

Both these energy filtering TEMs first form an unfiltered diffraction pattern (or image) then the magnetic prism transforms the pattern into an electron energy loss spectrum, where a specific part of the spectrum is selected by an energy selecting slit. Finally, the selected electrons are transformed back into an energy filtered diffraction pattern (or image) by means of an electron optical transfer system and the pattern is recorded with a slow scan CCD camera.

Both types are operated in a very similar manner: to form an energy filtered pattern (in which the intensity originates only from electrons within a selected energy range) the energy loss spectrum is shifted relative to an energy selecting slit. This slit is positioned after the prism but before the final lens system and its width can be varied between 5 and 60 eV, thus determining the energy window for the diffraction pattern. The zero loss peak of a spectrum is adjusted to lie on the optical axis.

The energy shift can be made by (i) increasing the acceleration voltage of the microscope by $+\Delta E$ to keep the energy loss of interest (ΔE) on the optical axis, or (ii) changing the current through a set of coils placed after the spectrometer magnet.

Furthermore, in both these microscopes an unfiltered diffraction pattern can be simply obtained by withdrawing the energy selecting slit. The effect of this on the resulting HOLZ line profiles will be discussed in Sect.4.

3.2 Advantages of energy filtering for CBED analysis

The angular width of a HOLZ line can be deduced from the expression for the intensity of a HOLZ reflection in the simplest two beam approximation by:

$$Ig = (\pi e^{-M}/\xi_g) \sin^2 (\pi t s')/ \pi s' \quad \text{with } s' = s^2 + \xi_g^2$$

where ξ_g is the extinction distance for the reflection g and e^{-M} is the Debye-Waller factor; $M=4\pi^2 g^2 \langle u^2 \rangle$, $\langle u^2 \rangle$ being the mean square atomic displacement due to thermal vibrations. From the previous equation, it is possible to determine the angular width $\Delta\Omega$ over which the diffracted intensity is appreciable:

$$\Delta\Omega = 2\, e^{-M}/g\xi_g \quad \text{for } t >> \xi_g /e^{-M}$$
$$\Delta\Omega = 2/gt \quad \text{for } t << \xi_g /e^{-M}$$

For a HOLZ reflection ξ_g /e^{-M} is of the order of 2000 nm and hence $\Delta\Omega \leq 10^{-4}$ rad.

Energy filtering is very important: the sharpness of the lines increases with increasing specimen thickness, but at the same time so does the probability of single or multiple inelastic plasmon losses. This leads to a broadening (due to the angular distribution of the plasmon loss electrons) and to a shifting of the intensity minimum of the HOLZ lines. Exciting a plasmon loss of a 15 eV at 100 (200) keV is equivalent to a relative change of 0.8 (0.4) x 10^{-4} in the angular position of a HOLZ line, which is comparable with $\Delta\Omega$. Although our previous results (see D5, D10) indicate that the HOLZ line shift in Si at 200 kV does not significantly alter the accuracy of the strain tensor determination, it is nonetheless important to eliminate this effect. This can be done by zero-loss filtering[3], even for very thick samples. It is important to note that the use of relatively thick specimen is recommended in CBED experiments, as it minimises the effects of thin film relaxation.

The effects of filtering on the quality of a pattern are evident in Fig. 3.1 below, where three patterns from an undistorted Si region are presented. The improvements

due to either filtering or cooling seem qualitatively the same, but a more careful inspection of the peaks indicates that the contrast is higher in the cooled pattern, whereas the line profile is narrower in the filtered one. In any case, the drawbacks mentioned in Section 2 suggest that working at room T with energy-filtering would be more convenient than with LN_2 cooling alone.

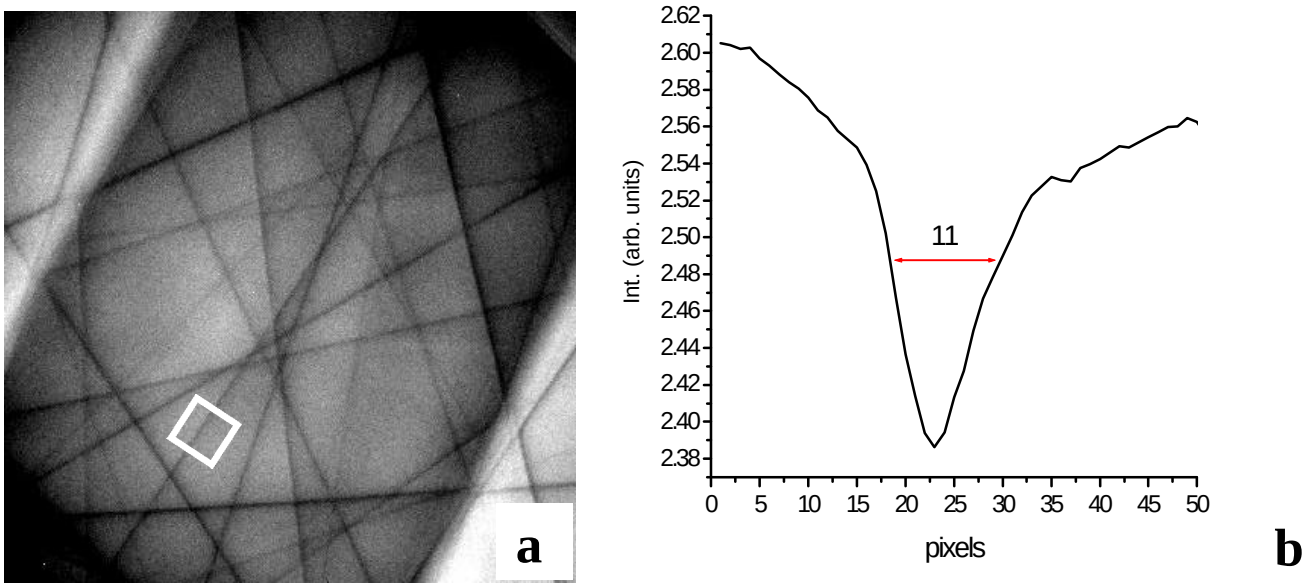

Fig. 3.1a,b – <230>, Room T unfiltered pattern from undistorted silicon **(a)** and intensity linescan across the marked HOLZ area **(b)**

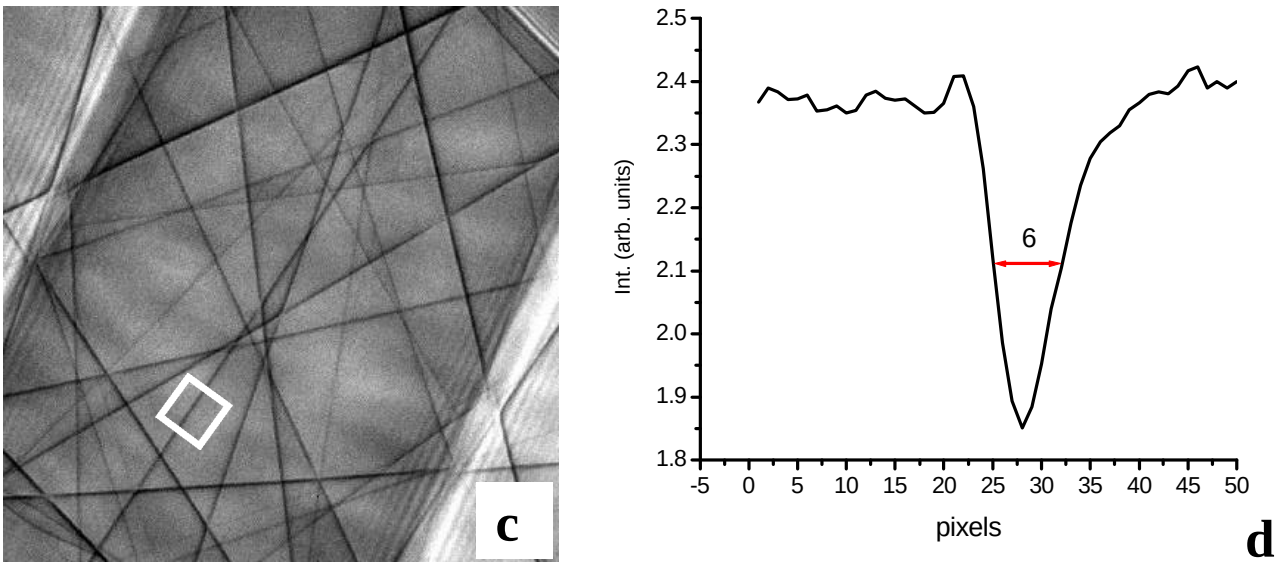

Fig. 3.1c,d – <230>, Room T energy- filtered pattern from undistorted silicon **(c)** and intensity linescan across the marked HOLZ area **(d)**

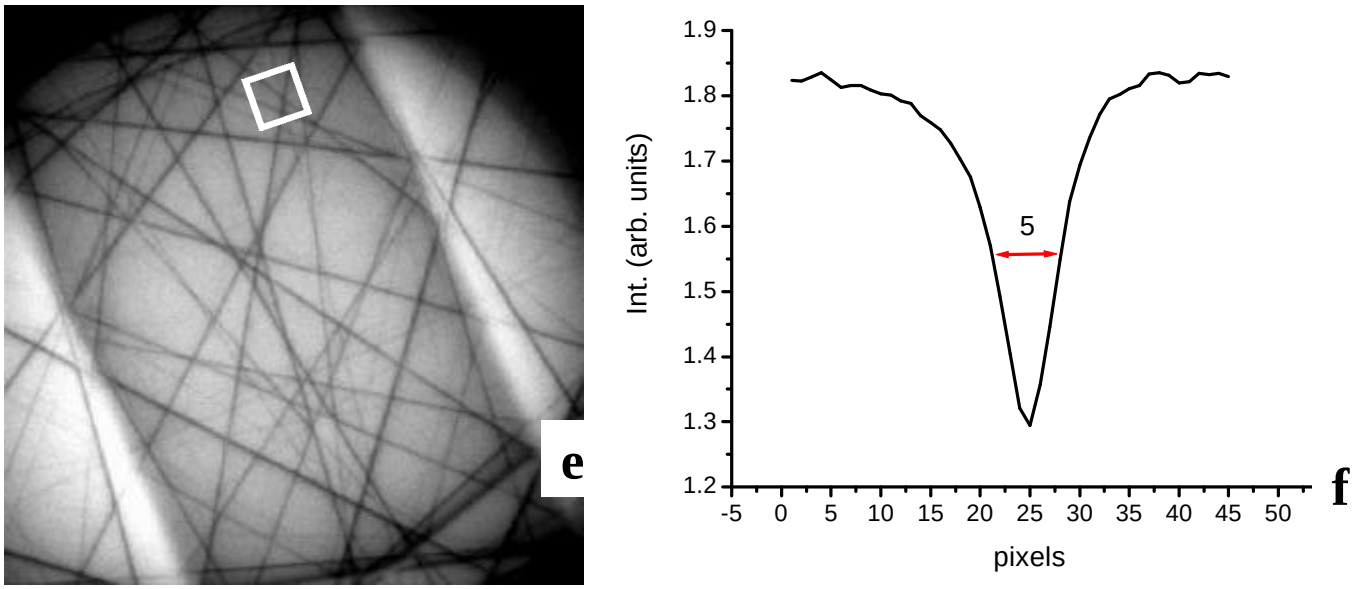

Fig. 3.1e,f – <230>, LN_2 T unfiltered pattern from undistorted silicon **(e)** and intensity linescan across the marked area **(f)**

4 Energy-filtering and sample preparation

For the reasons discussed above, working at room T would be preferable for our type of analysis. The use of a GIF or of an in-column filter greatly helps in this sense, as it allows one to filter out all inelastic components from the patterns, including the contributions from the contamination, and therefore increases the S/N ratio.

Room T CBED work is also possible without any filtering, but in this case it becomes imperative to ensure a very high vacuum within the column and an extremely clean sample, to avoid any contamination that would blur the pattern. The latter point can be considerably improved by plasma-cleaning the sample surface prior to TEM analysis. This system applies a low-energy, high frequency (HF) plasma to effectively clean the specimen's surface without changing its elemental composition or structural characteristics. The plasma is created within a chamber, in which the sample holder is inserted, by an oscillating electromagnetic field that excites gas atoms. The impinging plasma ions impact the surface with energies typically lower than ~ 20 eV. Cleaning is carried out through the formation of reactive gas compounds that chemically interact with carbon-based materials on the specimen and

specimen holder. An example of the Fischione Model 2010 Plasma Cleaner available at USFD is shown in Fig. 4.1 below.

Fig. 4.1 – Fischione Model 1020 Plasma Cleaner

Also, when room T analysis is performed, the analysis time for each point must be minimised, since the longer the beam impinges on the surface the more contamination accumulates. This means that the beam positioning should be as fast as possible, and the shortest acquisition time, compatibly with the quality of the pattern, used. The former will be achieved with the automatic beam positioning system of AnalySIS, whereas the latter depends on the intensity of the electron spot.

In the specific case of the memory cell devices, like those analysed within the 3rd Campaign, however, a further obstacle (of geometric nature) makes it difficult to work at room T with no filtering. The typical devices would look like those sketched in Fig. 4.2, where the arrow indicates the directions of the electrons through the sample thickness.

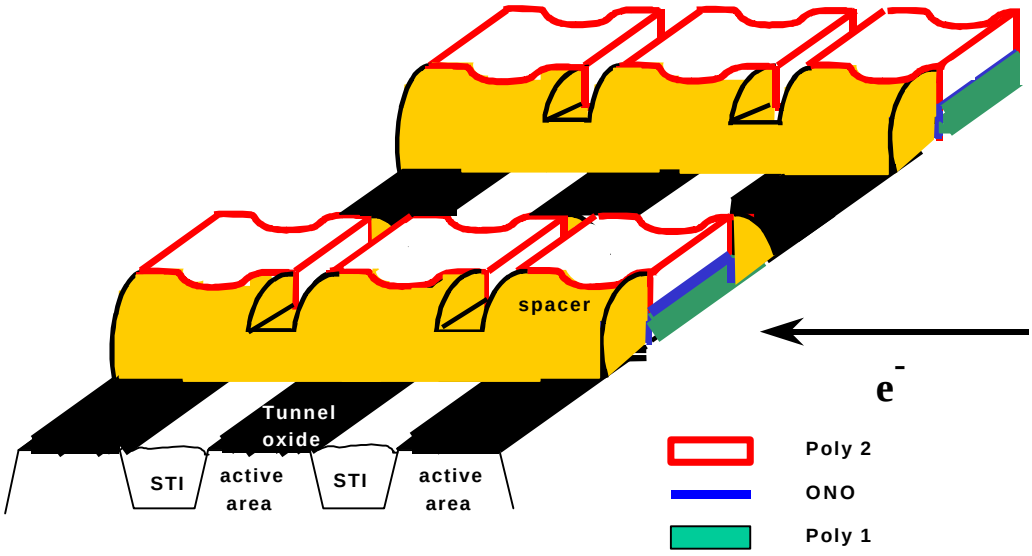

Fig. 4.2 – A sketch picturing the typical devices of the morphological run within the 3rd campaign.

An ideal cross-section for CBED analysis would look like the one represented in

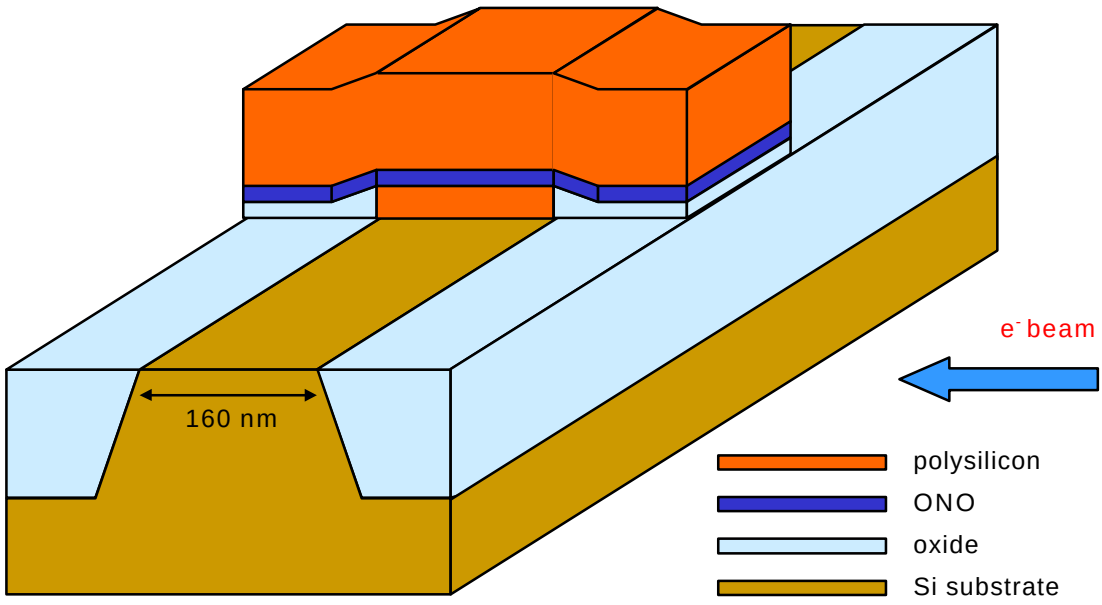

Fig. 4.3 Scheme of an ideal cross-section of the devices of the 3rd campaign. The thinning direction is now perpendicular to the STI direction.

Fig. 4.3. It must be noted that now the analysis is performed in a direction which is perpendicular to the STI structures. While travelling through the sample, the incident

electrons first penetrate in the oxide region, then in the silicon active region and eventually, after crossing another oxide region, emerge from the exit surface. It is clear that, independently from the total sample thickness, the volume of silicon crystal for the generation of the CBED pattern is determined only by the active area length, which is 160 nm in the upper region of the structures analysed in 3rd campaign.

Since the typical sample thickness used so far for CBED analysis ranges from 200 to 300 nm, the first consequence of the reduces crystal volume is a degradation of the diffraction pattern quality, as it can be seen in Fig. 4.4. It must be said that an

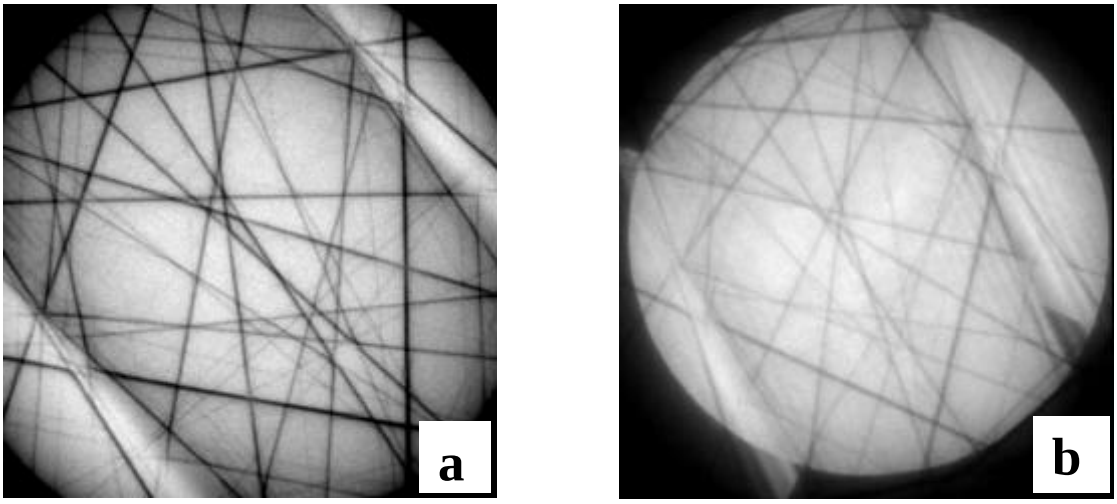

Figure 4.4 <230> CBED patterns taken in perfect silicon, in regions of (a) about 300 nm and (b) less than 200 nm thick. The magnification is slightly different in the two images.

active area 160 nm wide generates patterns which are still workable with the AnalySIS software. On the other hand, it is expected that a further reduction in the structure dimension will rapidly push the CBED technique toward its physical dimensional limit, which can be expected to be at about 100 nm, as confirmed by dynamical CBED pattern simulation (see Fig. 4.5)

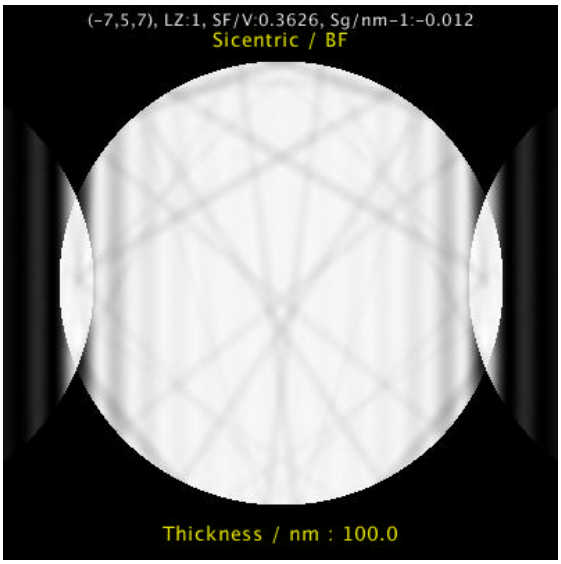

Figura 4.5 Simulated CBED pattern of <230> Si, 200 kV, 100 nm thick.

using the commercial software package JEMS[4]. Here, the HOLZ lines are barely visible.

The particular sample geometry requires additional care in the specimen preparation. The main difficulty is that, using conventional TEM specimen preparation, it is not possible to monitor all the preparation steps using the optical microscopes. Fig. 4.6 represents a typical unwanted result in the specimen preparation due to the

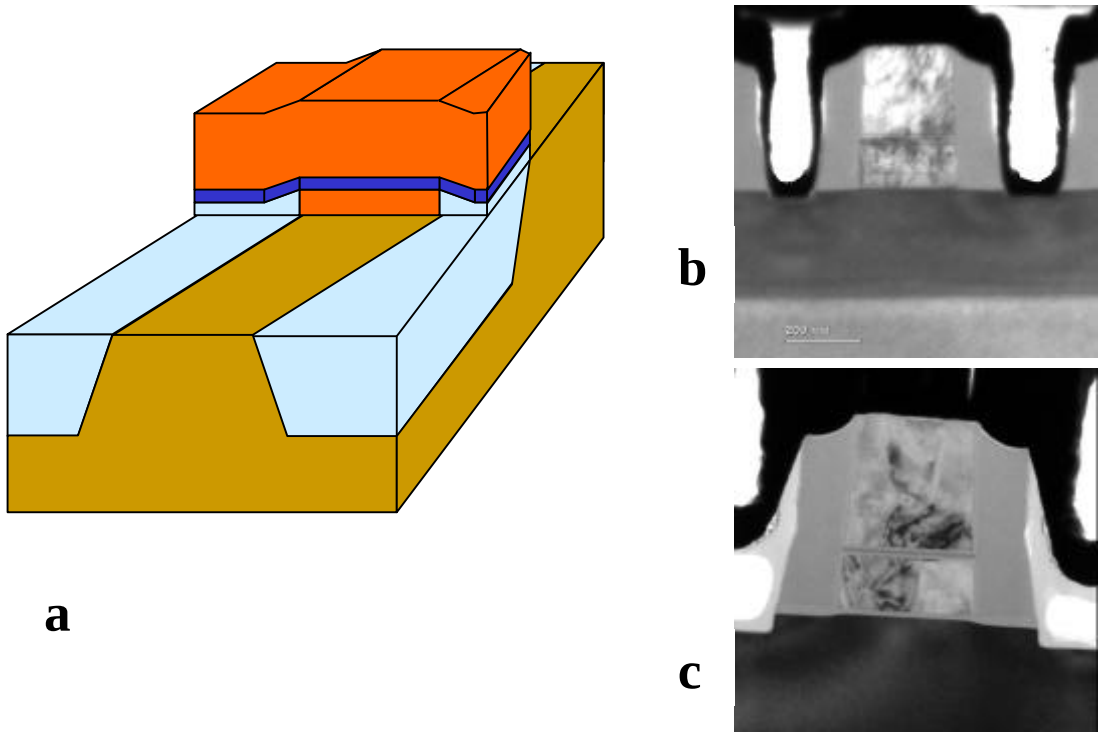

Fig. 4.6 a) Misalignment of the thinning plane with respect to the STI stripe direction. In some regions a superposition of crystalline Si and silicon oxide occurs, as in the image b), while in other, thinner regions (see c)) only the silicon active area is visible.

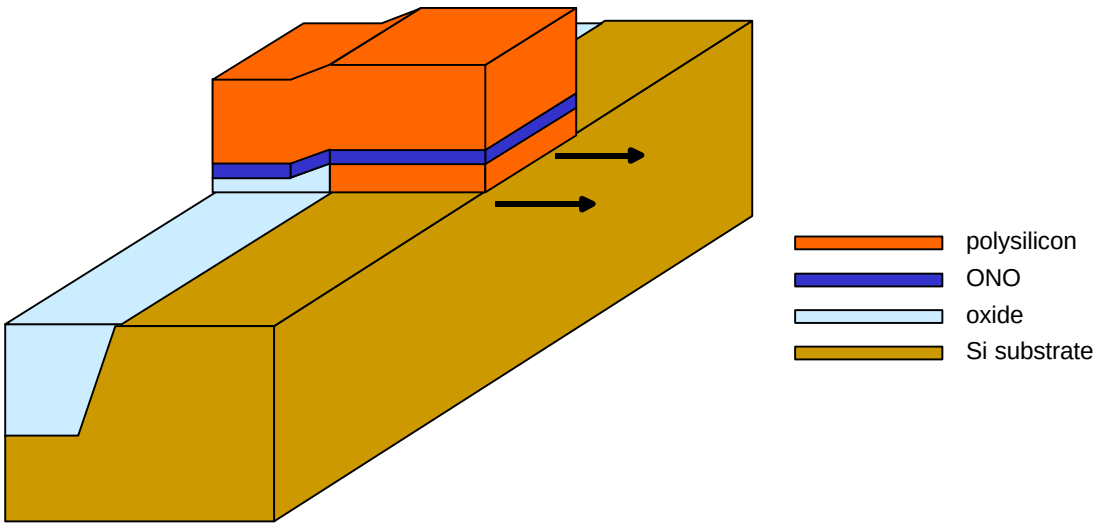

Fig. 4.7 The complete removal of the oxide region can allow a strain relaxation in the active area along the direction perpendicular to the surface (arrowed).

misalignment of the thinning surface with respect to the STI stripes direction. In this case, it can be difficult to state if the specimen is well prepared, i.e. the active area is 'embedded' between two oxide regions, simply by inspecting the corresponding image.

Another important situation is represented in Fig. 4.7. In this case the silicon oxide region has been completely removed at one surface (which can either be the upper or the lower one). There are two main drawbacks in this configuration: first, there can be a considerable reduction in the total volume of crystalline silicon available for the measurement; second, strain relaxation is expected to occur at the silicon free surface, so that the volume of silicon with 'bulk' strain properties (i.e. the volume of homogeneously strained silicon which can generate a good quality CBED pattern) is further reduced. It must be noted that, in most cases, these unwanted configurations cannot be detected in the TEM images: when the specimen shows the contrast typical of a crystalline silicon and a superimposed oxide (se for example Fig. 4.3 b)) it is not possible to determine if the oxide is at the upper, lower or both surfaces.

From these simple considerations it turns out that an ideal specimen should be prepared as the one represented in Fig. 4.3, in which the whole active region volume is packed between two silicon oxide regions. Although the oxide regions degrade the diffraction pattern quality by introducing a diffuse scattering, which contributes essentially to the background intensity, they also prevent strain relaxation within the silicon at the free surfaces. Since the energy filtering enhances the S/N ratio of the diffraction patterns, its use is recommended to reduce the mentioned effect in the CBED analyses of cell structures at room temperature.

4.1 The Focused Ion Beam (FIB) for TEM sample preparation

The difficulties in the specimen preparation discussed above can be overcome only by using a Focused Ion Beam (FIB) for the specimen preparation.

A FIB workstation operates in a way similar to a scanning electron microscope (SEM) in that both instruments take charged particles from a source, focus them into a beam through electromagnetic/electrostatic lenses, and then scan across small areas of the sample using deflection plates or scan coils.

The key difference between the two instruments is that, instead of using electrons to form its imaging beam, the FIB uses gallium ions from a field emission liquid metal

ion source. Within reasonable beam currents an electron beam is nondestructive, but since gallium ions are much heavier than electrons, a FIB's ion beam mills the sample surface as it images it. With its computer controlled 5 axis stage, a focused ion beam workstation is, in effect, a milling machine on a micro scale. However, imaging the region of interest of the sample induces amorphisation of the unprotected edges, which would adversely affect the strain field distribution in the final cross section for the TEM/CBED analysis.

For this reason, to perform the strain analysis of our cell structures, the samples have been thinned using a Dual Beam equipment. A Dual Beam is an instrument in which both ion (FIB) and electron (SEM) columns are present. The FIB column is used to thin the sample, whereas the SEM column is used to image it during thinning with high resolution and no damage. The equipment available at STMicroelectronics and employed for cross sectioning the samples of the cell structures for 0.15 μm NVM applications is shown in Fig. 4.8.

Fig.4.8. The FIB dual beam instrument FEI Strata DB 235, used for the preparation of TEM cross sections of the 2D cell structures

The samples have been manually pre-thinned down to a thickness of about 30 μm. As the purpose is strain measurement, no protective layer could be deposited in line. On the other hand, the regions of interest cannot be directly exposed to the ion beam. Therefore, in order to avoid the surface damage during the ion-beam assisted

W deposition in the dual beam, a 80 nm thick Au layer has been sputtered on the samples prior to insertion of the sample in the Dual Beam chamber. This layer has a very poor adhesion to the surface, and does not induce further stress in the silicon substrate.

As mentioned, the advantage of the Dual Beam over the conventional FIB is that the job in progress can be observed with the electron beam, thus avoiding the section damage due to ion implantation. In this case, due to the geometry of the structures of interest, it has been necessary to look carefully for the point where the trench sides start to appear, and to stop there the ion beam sectioning, at both sides of an active area. The availability of the electron beam to monitor this feature has proved to be decisive for the success of the preparation procedure.

Conclusions

During the STREAM activity, a lot of experience has been acquired about the way both the electron source characteristics and the operating conditions of the electron microscopes available in the Consortium affect the quality of the CBED patterns and, in turn, the accuracy of the strain analysis.

The main results can be summarised as follows:

- The use of a 1 nm beam spot is recommended when regions with large strain gradients are to be analysed
- Although tiny spots can be achieved also with thermionic electron guns, FEG sources are more convenient, as their much higher brightness (100-1000x) allows higher beam intensities and in turn reduces the acquisition times
- Using the smallest spot implies higher contamination problems in the probed area of the investigated sample. This problem can be minimised by cooling the sample to a temperature of about 100 K, which is accomplished by using liquid nitrogen cooled sample holders. However, working at room temperature is not only experimentally easier (the normal double tilt holders are mechanically simpler and more stable), but also avoids the problems related to the difference in the dilatation coefficient of the various materials which the structure consists of.
- The best compromise is therefore working at room temperature with a beam positioning capability, which allows the microscope to be operated in diffraction mode, without checking the spot position at each CBED pattern acquisition step.

  Also, an energy-filtering system to minimise inelastic scattering effects is recommended for analysis of sub-quarter-micron devices.
- Working at room T reduces the dwell time of the electron beam in a specific location of the sample. The final version of the SIS STREAM software, which makes the beam positioning an automatic procedure, is the key feature of the strain analysis work in the test structures for non volatile memories investigated during the project activity and, in general, in the even shrinking devices of the present and future microelectronics.

APPENDIX I

Choice of a zone axis suitable for CBED experiments on [001] sections of silicon

If silicon plan sections or cross sections of vertical transistors have to be analysed, the direction perpendicular to the surface of the specimen is a <100> one. For the strain determination by TEM/CBED, the zone axes so far employed for the structures investigated during the STREAM activity are no more convenient. The <230> zone axis is 33.7° off the <100> projection, whereas the <130> is closer, but still needs a

A more suitable choice can be the <150> zone axis, which in cubic crystals like silicon is just 11.3° off the <100> direction; this is the same angle that the now commonly used <230> axis makes with the <110> direction, which is the perpendicular to the cross section plane of the structures patterned in the silicon fabrication technology.
To implement a new zone axis into the AnalySIS software, the following topics are to be considered:

- Choice of the acceleration voltage. For the reasons mentioned in Deliverable D10, the most suitable one is 200 kV. In fact, it is the typical maximum voltage of modern TEMs, and it allows higher beam brightness and thicker analysable sample regions with reduced relaxation problems
- Presence of an adequate number of kinematical HOLZ lines in the central disk of the CBED pattern

To start the investigation, a <150> CBED pattern has been taken in an undeformed region of a silicon cross section, tilted 11.3° off the <110> orientation. The arrangement of the HOLZ lines in the central disk of such a pattern is visible in Fig.A1a). In the central region bounded by the strong dynamical 400 reflections of the ZOLZ, a number of HOLZ lines with an adequate contrast and apparently free of dynamical interactions are visible. This behaviour has been checked with a full dynamical simulation, based on the Bloch wave theory, by the above mentioned commercial software package JEMS[3]. It has been assumed a sample thickness of 260 nm and a deviation parameter large enough to include the relevant HOLZ lines present in the experimental CBED pattern. The image so obtained is reported in Fig.A1b). The similarity between the two patterns is striking and the 10 HOLZ lines which are both continuous and not subject to significant deviations from linearity

when interacting with the strongly dynamical lines of the ZOLZ, are selected for the strain analysis by the SIS software.

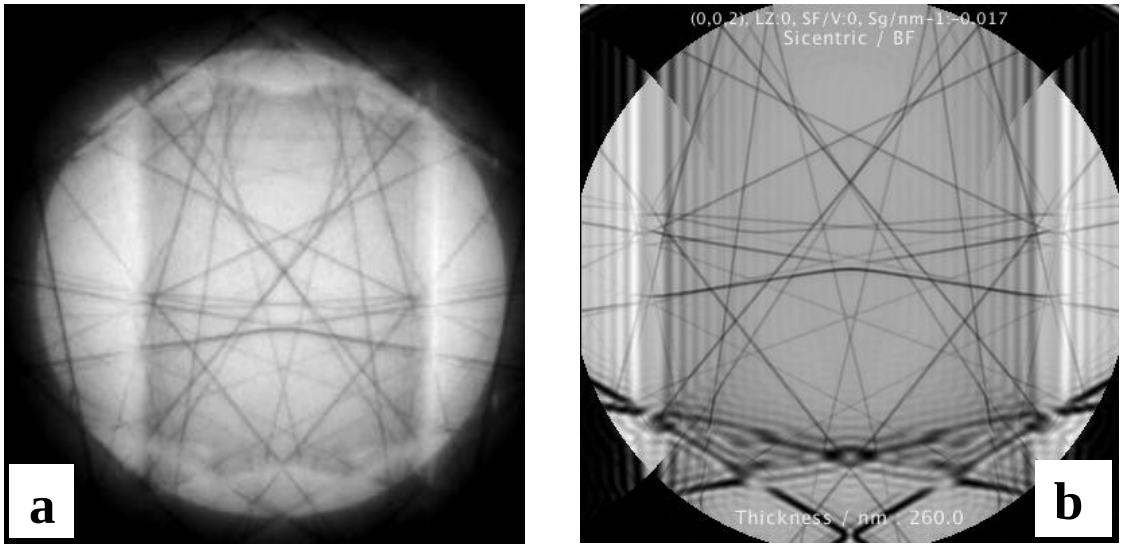

Figure A1. A) Experimental CBED pattern taken at 200 kV in the <150> orientation. The sample is undeformed silicon, cooled to 100 K; b) Corresponding full dynamical simulated pattern (JEMS software) for t=260 nm. The magnification and the convergence of the incident beam is different in the two patterns, but the arrangement of the HOLZ lines is quite well reproduced in the simulation.

The resulting skeletonisation by AnalySIS of these 10 lines is visible in Fig.A2. The coloured straight lines fit very well the experimental HOLZ lines.

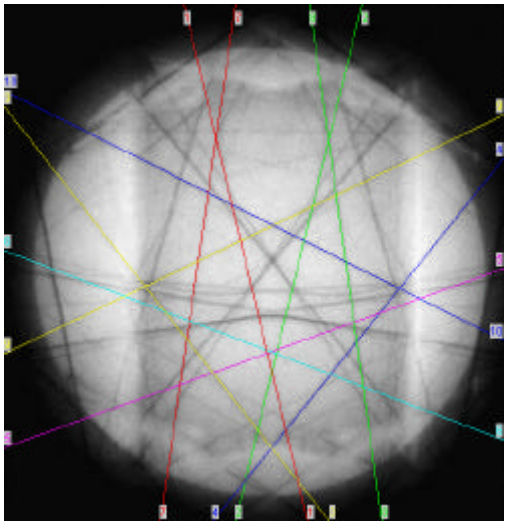

Fig.A2. Skeletonisation of the experimental CBED pattern in Fig.A1, as obtained by the SIS software

For a preliminary investigation of the applicability of this set of lines to the strain analysis in plan sections or vertical transistors, only 10 crossing points between

HOLZ pairs have been chosen, whereas the number of distances between these points has been limited to 21. The effective voltage is deduced from the HOLZFIT programme, included into this software (see Deliverables D10 and D13), assuming the lattice parameters of silicon at a temperature of 100 K (a=0.5429 nm). The value so obtained is 198.63 kV and the match between experimental and kinematically simulated sets of distances is quite good, as deduced from the χ^2 value. In Table A1 are reported the first 9 values of the calculated effective voltages, in increasing order of χ^2. These values are comparable to those obtained for the simulation in the standard <230> projection.

Table A1. Effective voltage of the TEM electron beam, obtained by the SIS software from the skeletonisation shown in Fig.A2. The value to be used in the simulation of deformed regions is the first in the output list (198.63 kV) i.e. the one with lowest χ^2-value

```
 Experimental CBED pattern of undeformed silicon taken in the <150>
orientation

 INCIDENT ELECTRON BEAM HIGH VOLTAGE   199.080000 KV
                       WAVELENGTH     0.025147 A
                       CAMERA LENGTH  8000.000000 MM

                    NEAREST ZONE AXIS    1   5   0

 Fitting Voltage   chi**2   Magnification

     198.630       0.6434         2.3351
     198.640       0.6436         2.3354
     198.620       0.6439         2.3347
     198.650       0.6446         2.3358
     198.610       0.6451         2.3344
     198.660       0.6462         2.3361
     198.600       0.6469         2.3341
     198.670       0.6485         2.3365
     198.590       0.6495         2.3337
```

- *Test of the kinematical character of HOLZ lines*. The next step in the evaluation of this zone axis is the assessment of the kinematical character of the HOLZ lines present in the central disk of the CBED pattern. This is accomplished by the same procedure described in Deliverable D10 for the standard <230> zone axis. Namely, a series of <150> CBED patterns have been dynamically simulated by JEMS for thickness ranging from 100 to 260 nm, including 219 beams in the Bloch wave formalism. This method is based on the known effect of the shift in

the position of a dynamical HOLZ line, as induced by a variation in the sample thickness. If this shift occurs, the simulation of this line, as performed by HOLZFIT, which is based on a kinematical approach, would be inaccurate. The simulated CBED patterns have been input to the SIS software, so to obtain the corresponding effective voltage. The results simulated for thickness 164, 196, 228 and 260 nm, which represent a reasonable experimental thickness range, are reported in Table A2. The voltage deviation is of only 10 Volt in this range, which indicates that the HOLZ lines selected for the strain analysis (Figure A2) can be considered to a good approximation as kinematical.

Table A2. Effective voltage and minimum χ^2 value for different sample thickness, calculated by applying the SIS software to the JEMS simulated <150> CBED patterns like that in Fig.A2

Sample thickness (nm)	Effective voltage (kV)	Minimum χ^2 value
164	199.98	0.635
196	199.98	0.625
228	199.98	0.869
260	199.99	0.590

Test on accuracy. As discussed in Deliverable D10 for the case of the <230> zone axis, the subsequent step in the evaluation of a zone axis is the assessment of the accuracy in the strain determination and the number of components of the strain tensor that can be determined from a single CBED pattern.

Likewise, in the case of the <150> zone axis, it has been simulated the same five sets of lattice parameters, which correspond to different amounts of strain. With respect to the calculations performed by EMS and reported in D10, now the computation time employed by JEMS is much shorter, as it neglects the many additional faint reflections, which originate from the decrease of crystal symmetry from diamond cubic to triclinic. However, as this test is just preliminary, the number of different structures has been limited to 5, yet the results are unambiguous.

In Table A3 are reported the lattice parameters deduced from the analysis, through the STREAM SIS software, of the CBED patterns simulated by JEMS assuming these five different structures (labelled Strained 1 through 5).

Table A3. Strained silicon lattice cells simulated by JEMS and STREAM SIS software. Δ is the difference between the parameters assumed as an input to JEMS and those deduced from the SIS programme.

Structure	**Parameter**	**a (Å)**	**b (Å)**	**c (Å)**	**α (deg)**	**β (deg)**	**γ (deg)**
	Simulated cell	5.424	5.424	5.434	89.98	90.02	89.89
Strained 1	Best fit	5.424	5.424	5.432	89.97	90.03	89.88
	Δ	0.	0.	0.002	0.01	0.01	0.01
	Simulated cell	5.426	5.426	5.434	89.98	90.02	89.94
Strained 2	Best fit	5.425	5.425	5.433	89.96	90.04	89.92
	Δ	0.001	0.001	0.001	0.02	0.02	0.02
	Simulated cell	5.425	5.425	5.433	89.98	90.02	89.92
Strained 3	Best fit	5.425	5.425	5.432	89.97	90.03	89.92
	Δ	0.	0.	0.001	0.01	0.01	0.
	Simulated cell	5.424	5.424	5.435	89.98	90.02	89.89
Strained 4	Best fit	5.422	5.422	5.433	89.98	90.02	89.86
	Δ	0.002	0.002	0.002	0.	0.	0.03
	Simulated cell	5.433	5.433	5.425	89.98	90.02	90.08
Strained 5	Best fit	5.432	5.432	5.422	89.98	90.02	90.06
	Δ	0.001	0.001	0.003	0.	0.	0.02

From Table A3 it comes out that the accuracy is quite good for all the lattice parameters. Both positive and negative variation in the *a,b* and *c* lattice parameters are well reproduced. On average the accuracy is about $2x10^{-3}$ Å ($2x10^{-4}$ nm) for *c* and still better for *a*. The angles α and β are reproduced with an average error of 0.01 degrees, which indicates that the sensitivity to shear strain in the (X,Z) and (Y,Z) planes is good; as to γ, its value is not independent, but related to the diagonal ε_{XX} component of the tensor, according to the plane strain approximation.

It can be concluded that the properties of the <150> zone axes at 200 kV are satisfactory, particularly from the viewpoint of kinematical character and strain sensitivity and accuracy of the HOLZ line pattern. As such, it can be applied to the

strain analysis of the structures of interest to the field of microelectronics other than those investigated during the project activity; they include the <001> plan sections and the vertical transistors.

APPENDIX II

CBED experiments on GaAs <110> cross sections in <230> orientation

As mentioned by T.Schilling (SIS) during the Second Review Meeting in Leuven, there is a request from the microelectronics community to analyse by TEM/CBED the strain field in different regions of GaAs based sub-micron devices. Therefore, it has been decided to perform a preliminary investigation of the applicability of the technique to the field of compound semiconductors, starting from GaAs, which is of relevant interest in the field of microelectronics, though at a much lesser extent than the silicon based devices. In addition, the implementation of the GaAs semiconductor into the SIS STREAM software will expand the potential market of this commercially available product, which is one of the main results of the project.

The lattice of GaAs is of the zinc-blende type, i.e. it is a silicon-like face-centred cubic, with one sublattice occupied by Ga atoms and the second sublattice occupied by As atoms. The lattice parameters are: $a=b=c=0.5652$ nm, $a=b=g=90°$.

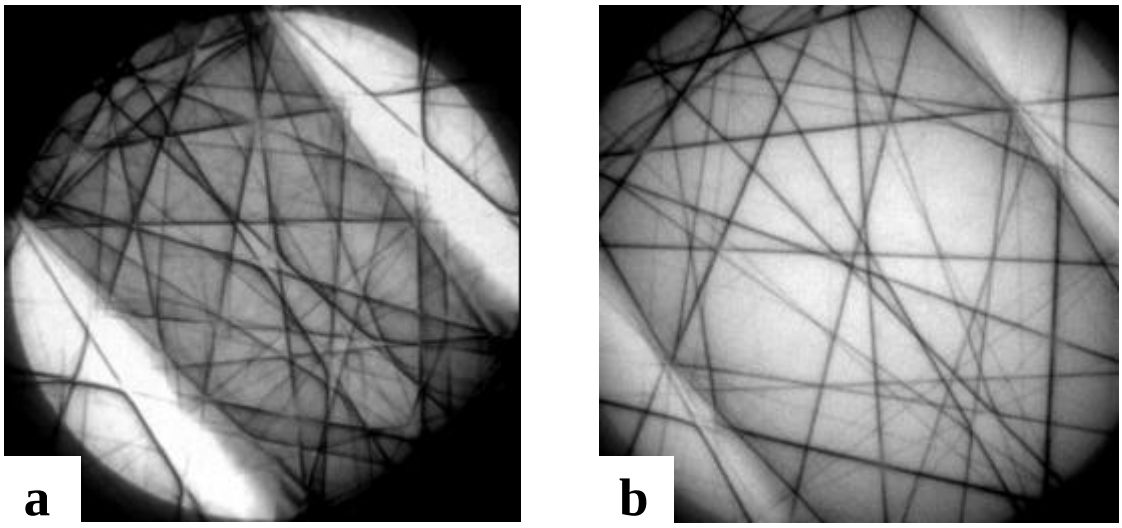

Figure A3. a) Experimental CBED pattern taken in an undeformed region of a GaAs cross section; b) Si CBED pattern taken in the same operating conditions, i.e. V=200 kV, <230> zone axis (see Deliverables D10 and D13).

The first step in the implementation of GaAs into the STREAM software is to include a GaAs.ini file with all the relevant data. Then the zone axis and the acceleration voltage need to be chosen. As the standard operating conditions for strain analysis include a <230> zone axis and a 200 kV acceleration voltage of the electron beam, they have been selected also for the GaAs case. Moreover, the same set of 18 HOLZ lines and of 38 distances between HOLZ intersection points have been assumed in the first instance. In Fig.A3a is reported an experimental CBED pattern taken in the undeformed region of a GaAs <110> cross sections, tilted to the <230>

zone axis. The pattern looks somewhat different from the corresponding one, taken in silicon, which is shown in FigA3b.

The skeletonised pattern superimposes to the experimental HOLZ lines fairly well (see Fig.4a). However, the quality of the fit can be better judged by running the software to get the effective voltage and checking the χ^2-test. The results are reported in Table A4.

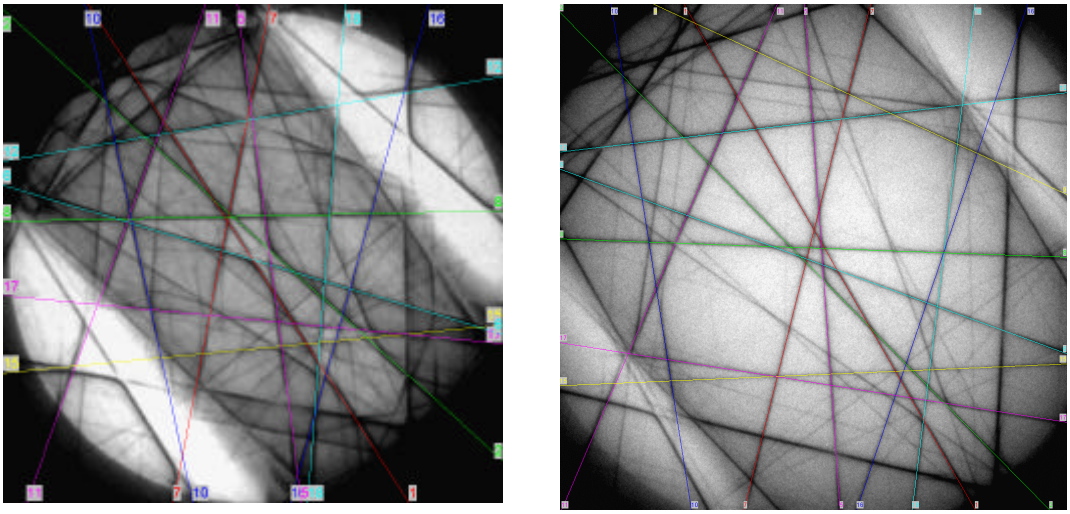

Figure A4. Skeletonisation of the CBED patterns in Fig.A3. a) GaAs; b) Si

Table A4. Effective voltage for undeformed GaAs, obtained by the SIS STREAM software. The best fit is found for a value of 198.35 kV.

Experimental undeformed GaAs, taken in the <230> zone axis

INCIDENT ELECTRON BEAM HIGH VOLTAGE 198.220000 KV
WAVELENGTH 0.025210 A
CAMERA LENGTH 8000.000000 MM

NEAREST ZONE AXIS 2 3 0

Fitting Voltage	chi**2	Magnification
198.350	1.5357	1.1567
198.340	1.5358	1.1569
198.360	1.5377	1.1564
198.330	1.5378	1.1571
198.370	1.5416	1.1562
198.320	1.5418	1.1574
198.380	1.5475	1.1560
198.310	1.5479	1.1576
198.390	1.5554	1.1558

It comes out from this Table that the minimum χ^2 value is about 1.5, which is higher than that found for the corresponding case of Si <230> (χ^2<1, see Deliverable D10), however it is still acceptable.

The situation is different if one performs the test of the kinematical character of the HOLZ lines, likewise in the previous zone axes (see Appendix I for <150>).

The CBED patterns in the <230> zone axis have been simulated by JEMS for the thickness range t=164-260 nm. As in the case of silicon, it is found that the HOLZ line definition improves with thickness. An example of image is given in Fig.A5a, which refers to the thickest simulated sample. It includes all the HOLZ lines which have been selected for the strain analysis of silicon in this zone axis (see Deliverable D13). The pattern is quite similar to the experimental one (Figs. A3 and A4), although the latter includes more beams, which are neglected in the simulation. As such, it can be skeletonised by the SIS STREAM software and the result is shown in Fig.A5b; the calculated HOLZ lines superimpose quite well to those generated from JEMS.

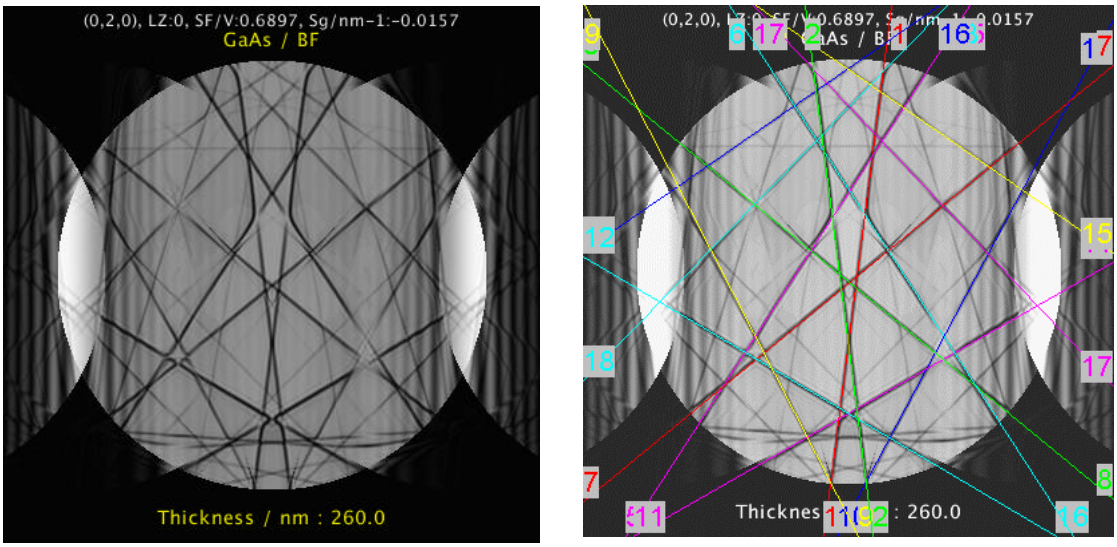

Fig. A5. (left) Example of simulated <230> GaAs CBED patterns, as obtained by JEMS. The thickness is t=260 nm. (right) Skeletonisation of the same pattern by the SIS software.

By comparing the JEMS-simulated and the experimental CBED patterns (Figs.A3a and A5a) it seems that the dynamical interactions between HOLZ lines are more severe in the former. This can be ascribed to the absorption effect, which is more pronounced in the experimental case, reducing the dynamical character of the experimental HOLZ lines. The minimum χ^2 values yielded by the SIS software are in the range of the unity in the whole thickness interval, which indicates that the HOLZ

lines, despite their mutual interactions, are reasonably well fitted by the corresponding kinematical ones. A few examples of χ^2 values and effective voltages for different sample thickness are reported in Table A5.

Table A5. Effective voltage and minimum χ^2 value for different sample thickness, calculated by applying the SIS software to the JEMS simulated <230> CBED patterns like that in Fig.A5.

Sample thickness (nm)	Effective voltage (kV)	Minimum χ^2 value
164	199.83	0.3944
196	199.49	0.7005
228	199.41	1.3041
260	199.45	0.7463

The data in this Table do not exhibit a clear voltage dependence on thickness, except for the value at t=164 nm. However, the voltage uncertainty is $2x10^{-4}$ if the first thickness value is neglected and $1.2x10^{-3}$ if it is taken into account. As usually the thickness of the sample region assumed to be undeformed and hence used for the effective voltage determination is different from the deformed ones, this voltage uncertainty sets a threshold for the minimum detectable strain in these conditions. This confirms that the interactions between the HOLZ lines selected for the strain analysis in the <230> CBED patterns of GaAs and the ZOLZ ones are significant. Nevertheless, it makes sense, within these limits, to perform the test of the strain sensitivity of this zone axis.

Test on the strain sensitivity. The set of 38 distances between crossing points for the 14 HOLZ lines in the <230> zone axis of GaAs, displayed in Figs. A4 and A5, must be sensitive to variations in the amount of strain present in the investigated active region of the structures; in fact, this has been already proved in the case of silicon. A quick, preliminary test is based on the equivalence between variations in the lattice parameter of silicon and variations in the accelerating voltage of the electron beam. As already mentioned in Deliverable D2, the Bragg law can be written in its small angle approximation (which holds for the electron energies typical of a TEM) as:

$$2d_{hkl}q = n\,l$$

where d_{hkl} is the interplanar spacing of the set of {*hkl*} planes, q is the Bragg angle of the corresponding reflection and l ($\mu V^{-1/2}$) is the wavelength of the electrons.

Differentiating this equation and taking into account that:

$$d_{hkl} = \frac{a}{\sqrt{h^2 + k^2 + l^2}}$$ (in a cubic crystal like silicon)

one gets:

$$\frac{\Delta a}{a} \propto \frac{\Delta V}{2V} \qquad (1)$$

This means that a variation in the TEM accelerating voltage affects the position of the HOLZ lines lines in the same way as a variation in the local lattice parameter (i.e. strain). As such, a number of CBED patterns can be taken in the same undeformed region of the TEM cross section for different beam voltages. One of these patterns (e.g. that taken at 200 kV) can be selected as the reference one and analysed by the STREAM SIS software to get the value of the effective voltage. The others can be treated as being originated from 'deformed' areas of the sample and processed by the software to get the strain tensor. In other words, this is equivalent to the case of analysing GaAs regions with varying amount of strain but at a fixed voltage.

In this preliminary text, we have taken CBED patterns at 200, 199.7, 199.4 and 198.8 kV. The resulting traces of the strain tensor are reported in Table A6.

The pattern taken at a nominal voltage of 200 kV has been analysed to yield the effective voltage (198.35 kV, see Table A4). The other patterns have been analysed as if they were originated from regions of 'unknown' strain.

Table A6. Values of the strain tensor trace obtained from experimental CBED patterns taken for decreasing acceleration voltages. This gives the same effect as a lattice change, which is computed by the SIS software. The effective voltage is deduced from the experimental pattern taken at 200 kV, i.e. V=198.35 kV (see Table A4).

CBED pattern #	Operating voltage (kV)	Corresponding tensor trace (x10^{-4})	Trace 3Δa/a from eq.(1)
1	199.7	-21	-22.5
2	199.4	-30	-45
4	198.8	-87	-90

The values of the traces are negative, in agreement with equation (1). This test shows that the HOLZ patterns are sensitive to deformation, at least in the 10^{-3} range. This result, together with the inaccuracy deriving from the dynamical character, indicates that in the conditions employed strains higher than 10^{-3} can be analysed

under the employed conditions. Of course, a check is necessary in samples with a known strain field distribution.

In conclusion, though promising, the extension to GaAs of the same procedure employed for Si (same set of HOLZ lines and distances in <230> zone axis) presently yields qualitative only strain information. To get quantitative data, possible improvements of the CBED procedure are:

- Use of the same zone axis, but with a different set of HOLZ lines and distances
- On the basis of the full dynamical calculations of this zone axis, introduction of a line-by-line correction of the HOLZ position
- Choice of a more suitable (less dynamical) zone axis

References

[1] A Armigliato, R Balboni, S Frabboni, A Benedetti, A G Cullis, G P Carnevale, P Colpani, G Pavia, *Mat. Sci. in Semic. Process*. **4** (2001), p. 97

[2] G.Kothleitner, TU Graz (Austria) (formerly with Gatan Inc., Pleasanton, USA; see also Ref. 1 in Deliv.D5)

[3] *Energy-Filtering Transmission Electron Microscopy* (L.Reimer Ed.) Springer-Verlag Berlin Heidelberg 1995, Ch. 6

[4] P.Stadelmann, Ultramicroscopy **21** (1987) 131. JEMS stands for Jawa Electron Microscopy Software, commercially available from the author.